Supplemental information

Summary of supplemental information

- **Supplemental methods** explain our method for Western blotting, flow cytometry, histology, cell sorting, RNA extraction, and cDNA library preparation for RNA sequencing.
- **Supplemental table1** lists reagents, genetically modified organisms and strains, cell lines, software, instrumentation, and source data used in this study.
- **Supplemental table2** lists gene sets which were only enriched in human ATL acute type samples, but not in CARD11(E626K)CD4 -Cre;HBZ Tg mice in the GSEA analysis.
- **Supplemental figure 1** shows strategies for targeting mutant mice.
- **Supplemental figure 2** shows Western blot analysis of splenic $CD4^+$ T cells from CARD11(E626K)$^{CD4\text{-Cre}}$ mice and *HBZ* Tg mice.
- **Supplemental figure 3** shows flowcytometric analysis of $CD4^+$ T cells, effector/memory T cells, and regulatory T cells in lymph nodes of mutant mice.
- **Supplemental figure 4** shows pathological analysis of lymph node and lung of mutant mice.
- **Supplemental figure 5** shows global gene expression profiling of effector/memory T cells obtained from mutant mice.
- **Supplemental figure 6** shows GSEA analysis of NF-κB canonical and non-canonical signaling pathway of mutant mice.
- **Supplemental figure 7** shows GSEA analysis of HBZ target genes of mutant mice.

Supplemental methods

Western blotting

Splenocytes from each mouse type (n = 2–3 for each type) were pooled between 8 months to 12 months after birth, then $CD4^+$ splenocytes were isolated using the mouse $CD4^+$ T-Cell Isolation Kit (Miltenyi Biotec, BG, Germany) and prepared for Western blotting. Total cell lysates were prepared as previously described [1]. Nuclear cell extracts were prepared using a Nuclear Extract Kit (Active Motif, CA, USA). Extracts were resolved by SDS-polyacrylamide gel electrophoresis, transferred to polyvinylidene difluoride nitrocellulose membranes, probed using the appropriate antibodies, and visualized by electrochemiluminescence (GE Healthcare, NJ, USA). The reagents used are listed in Supplemental table 1.

Flow Cytometry

Tissues were processed into single-cell suspensions and treated with red blood cell lysis buffer, and cells were transferred into phosphate-buffered saline containing 2% fetal bovine serum. The cells were blocked with Fc-block (BD Biosciences, CA, USA), stained with antibodies for 30 min at 4 °C, washed, and analyzed using a FACSCalibur Flow Cytometer (BD Biosciences), FACSCanto II Flow Cytometer (BD Biosciences), and FlowJo software (Tree Star, Inc., OR, USA). Antibodies used are listed in Supplemental table 1.

Histology

Mouse organs were obtained from 6 and 12 months after birth (n = 5, in each type of mice) and fixed in 4% paraformaldehyde and paraffin embedded. Sections were stained with hematoxylin and eosin (HE). For immunohistochemistry, sections were stained with the appropriate primary and secondary antibodies. Antibodies used are listed in Supplemental table 1.

Cell sorting, RNA extraction, and cDNA library preparation for RNA sequencing

Splenocytes from each mouse type (n = 3 for each type) at 4 to 6 months after birth were stained with FITC Anti-CD4, PE Anti-CD8, APC Anti-CD25, and 7-AAD for sorting of $CD4^+CD8^-CD25^+$ Treg, and with FITC Anti-CD4, PE Anti-CD44, APC Anti-CD62L, and 7-AAD for sorting of $CD4^+CD44^+CD62L^-$ Tem, and then sorted with a FACSAria II cell sorter (BD Biosciences). Total RNA was extracted using Isogen

(Nippon Gene, Tokyo, Japan), and cDNA was synthesized using the SMARTer Pico PCR cDNA Synthesis Kit (Clontech, CA, USA). Double-stranded cDNA was fragmented, and cDNA libraries were generated using the KAPA HyperPlus Library Preparation Kit (KAPA Biosystems, MA, USA) and FastGene Adapter Kit (Nippon Genetics, Tokyo, Japan). Sequencing was performed using NextSeq500 (Illumina, CA, USA) with a single-read sequencing length of 76 bp. Kallisto (version 0.43.1) was used for determining read counts and calculating transcripts per million[2]. edgeR (version 3.12) and iDEP (version 0.92) were used for statistical analysis [3,4]. R (version 4.0) and the Heatmap.2 function from the gplots package were used for creating heatmaps. Gene set enrichment analysis (GSEA) was performed using Molecular Signatures Database (MSigDB)–curated gene sets (KEGG, HALLMARK, GO biological process, and REACTOME gene sets) and Lymphoma/Leukemia Molecular Profiling Project (LLMPP)–curated gene sets [5-7]. False discovery rate (FDR) q-values ≤0.25 were considered significant. The reagents, data sets, and software used are listed in Supplemental table 1.

References

1. Shide K, Shimoda HK, Kumano T, et al. Development of ET, primary myelofibrosis and PV in mice expressing JAK2 V617F. *Leukemia*. 2008;22(1):87-95.
2. Bray NL, Pimentel H, Melsted P, Pachter L. Near-optimal probabilistic RNA-seq quantification. *Nat Biotechnol*. 2016;34(5):525-527.
3. Robinson MD, McCarthy DJ, Smyth GK. edgeR: a Bioconductor package for differential expression analysis of digital gene expression data. *Bioinformatics*. 2010;26(1):139-140.
4. Ge SX, Son EW, Yao R. iDEP: an integrated web application for differential expression and pathway analysis of RNA-Seq data. *BMC Bioinformatics*. 2018;19(1):534.
5. Subramanian A, Tamayo P, Mootha VK, et al. Gene set enrichment analysis: a knowledge-based approach for interpreting genome-wide expression profiles. *Proc Natl Acad Sci U S A*. 2005;102(43):15545-15550.
6. Liberzon A, Birger C, Thorvaldsdottir H, Ghandi M, Mesirov JP, Tamayo P. The Molecular Signatures Database (MSigDB) hallmark gene set collection. *Cell Syst*. 2015;1(6):417-425.
7. Staudt lab. Signature database. https://lymphochip.nih.gov/signaturedb/.

Supplemental table 1. The reagents, genetically modified organisms and strains, cell lines, software, instrumentation, and source data.

REAGENT or RESOURCE	SOURCE	IDENTIFIER
Experimental Models: Cell line		
Human: Su9T	Dr. K. Morishita, University of Miyazaki	N/A
Experimental Models: Organisms/Strains		
Mouse: C57/BL/6 *CD4*-Cre Tg	The Jackson lab	#022071
Mouse: C57/BL/6 CARD11(E626K)$^{stop FL}$	This paper	N/A
Mouse: C57/BL/6 CARD11(E626K)$^{CD4\text{-}Cre}$	This paper	N/A
Mouse: C57/BL/6 *HBZ* Tg	This paper	N/A
Mouse: C57/BL/6 CARD11(E626K)$^{CD4\text{-}Cre}$;*HBZ* Tg	This paper	N/A
Oligonucleotides		
Forward primer for *Card11* E626K: 5'-AAGACCATCTGGGTGGACGA-3'	This paper	N/A
Forward primer for wild-type *Card11*: 5'-CCGCCTCGGAGTATTTTCCA-3'	This paper	N/A
Reverse primer for mutant and wild-type *Card11*: 5'-TGCCAATGCTCTGTCTAGGG-3'	This paper	N/A
Recombinant DNA		
See Supplemental figure 1	This paper	N/A
Antibodies for Western blotting		
Rabbit Anti-CARD11 (1D12)	Cell Signaling Technology	#4435, RRID:AB_2070359
Mouse Anti-HA MoAb HRP conjugated (CARD)	Wako	#011-21911
Rabbit Anti-Phospho-CARD11 (Ser652)	Cell Signaling Technology	#5189, RRID:AB_10621241
Rabbit Anti-Cleaved BCL10	Dr. D. Morishita, Chordia Therapeutics	N/A
Rabbit Anti-Bcl10 (C78F1)	Cell Signaling Technology	#4237, RRID:AB_2228005
Mouse Anti-Phospho-IκBα (Ser32/36)	Cell Signaling Technology	#9246, RRID:AB_2267145
Rabbit Anti-Phospho-NF-κB p65 (Ser536)	Cell Signaling Technology	#3033, RRID:AB_331284
Rabbit Anti-NF-κB2 p100/p52	Cell Signaling Technology	#4882, RRID:AB_10695537
Rabbit Anti-NIK	Cell Signaling Technology	#4994, RRID:AB_2297422
Rabbit Anti-β-Actin (13E5) HRP conjugated	Cell Signaling Technology	#5125, RRID:AB_1903890
Goat Anti-Rabbit IgG HRP linked (secondary antibody)	Cell Signaling Technology	#7074, RRID:AB_2099233
Sheep Anti-Mouse IgG HRP linked (secondary antibody)	GE Healthcare	#NA9310V
Rabbit Anti-HBZ	Dr. Oshima, Tokushima Bunri University	Muraki et al. Oncogene 33, 2317–2328 (2014).
Mouse Anti-FLAG M2	MERCK	#F1804-50UG
Antibodies for flow cytometric analysis and cell sorting		
Rat FITC Anti-Mouse/Human CD11b (Mac1)	BioLegend	#101206, RRID:AB_312789
Rat FITC Anti-Mouse CD41	BioLegend	#133903, RRID:AB_1626237
Rat FITC Anti-Mouse CD3	BioLegend	#100204, RRID:AB_312661
Rat FITC Anti-Mouse CD4	BioLegend	#100406, RRID:AB_312691
Rat PE Anti-Mouse Ly-6G/Ly-6C (Gr-1)	BioLegend	#108408, RRID:AB_313373
Rat PE Anti-Mouse Ter119	BioLegend	#116208, RRID:AB_313709
Rat PE Anti-Mouse CD4	BioLegend	#100408, RRID:AB_312693
Rat PE Anti-Mouse/Human CD45R/B220	BioLegend	#103208, RRID:AB_312993
Rat PE Anti-Mouse/Human CD44	BioLegend	#103008, RRID:AB_312959
Rat APC Anti-Mouse CD8a	BioLegend	#100712, RRID:AB_312751
Rat APC Anti-Mouse CD62L	BioLegend	#104412, RRID:AB_313099
Rat APC Anti-Mouse CD25	BioLegend	#102012, RRID:AB_312861
Rat Anti-Mouse CD16/CD32 (Mouse BD Fc Block)	BD Biosciences	#553141, RRID:AB_394656
7-AAD Viability Staining Solution	BioLegend	#420404
Antibodies for immunohistochemistry		
Rabbit Anti-Mouse/Rat/Human CD3	Abcam	#ab16669, RRID:AB_443425
Rat Anti-Mouse CD45R (B220)	BD Biosciences	#550286, RRID:AB_393581
Rabbit Anti-CD44	proteintech	#15675-1-AP, RRID:AB_2076198
Rat Anti-Mouse/Rat FOXP3	eBioscience	#14-5773-82
Rat Anti-Mouse F4/80	BMA BIOMEDICALS	#T-2028, RRID:AB_1227366
Rabbit Anti-Mouse/Human Ki-67	Abcam	#ab15580, RRID:AB_443209
Goat Anti-Rabbit Immunoglobulins Biotinylated	Thermo Scientific	#31820, RRID:AB_228340
Critical commercial assays		
Mouse $CD4^+$ T Cell Isolation Kit	Miltenyi Biotec	#130-104-454
Nuclear Extract Kit	Active Motif	#40410
Deposited Data		
Gene expression datasets obtained from mouse samples	This paper	Not deposited yet
Gene expression datasets obtained from human samples	Kataoka et al., 2015	EGAD00001001411
Software and Algorithms		
FlowJo v10.7.1	FlowJo, LLC	http://www.flowjo.com/
Kallisto v0.43.1	Bray et al., 2016	http://pachterlab.github.io/kallisto/
GSEA v4.1.0	Broad institute	https://software.broadinstitute.org/gsea/
MSigDB	Broad Institute	http://www.gsea-msigdb.org/gsea/msigdb/index.jsp
Signature DB	NIH	https://lymphochip.nih.gov/signaturedb/
R version 4.0.3	R Core Team	www.r-project.org
edgeR v3.12	Robinson et al., 2010	https://bioconductor.org/
iDEP v0.92	Ge et al., 2018	http://bioinformatics.sdstate.edu/idep/

Supplemental table 2. Gene sets which were only enriched in human ATL acute type samples, but not in CARD11(E626K)CD4-Cre;HBZ Tg mice.

pathway_name	human comparison	human NES	human FDR	mouse comparison	mouse NES	mouse FDR
KEGG_ASCORBATE_AND_ALDARATE_METABOLISM	Acute ATL vs. Healthy	1.869	0.010	Compound vs. WT	0.879	0.677
KEGG_LINOLEIC_ACID_METABOLISM	Acute ATL vs. Healthy	-1.700	0.051	Compound vs. WT	-0.737	0.994
KEGG_PORPHYRIN_AND_CHLOROPHYLL_METABOLISM	Acute ATL vs. Healthy	1.748	0.054	Compound vs. WT	1.136	0.338
KEGG_RIBOFLAVIN_METABOLISM	Acute ATL vs. Healthy	1.552	0.151	Compound vs. WT	-0.824	0.987
KEGG_REGULATION_OF_AUTOPHAGY	Acute ATL vs. Healthy	1.564	0.158	Compound vs. WT	0.984	0.521
KEGG_ALANINE_ASPARTATE_AND_GLUTAMATE_METABOLISM	Acute ATL vs. Healthy	1.477	0.195	Compound vs. WT	-0.904	1.000
KEGG_PENTOSE_AND_GLUCURONATE_INTERCONVERSIONS	Acute ATL vs. Healthy	1.632	0.200	Compound vs. WT	1.101	0.392
KEGG_BIOSYNTHESIS_OF_UNSATURATED_FATTY_ACIDS	Acute ATL vs. Healthy	1.458	0.202	Compound vs. WT	1.055	0.442
KEGG_GLYCEROLIPID_METABOLISM	Acute ATL vs. Healthy	1.444	0.203	Compound vs. WT	-0.911	1.000
KEGG_CARDIAC_MUSCLE_CONTRACTION	Acute ATL vs. Healthy	1.432	0.212	Compound vs. WT	0.953	0.554
KEGG_MELANOMA	Acute ATL vs. Healthy	1.383	0.213	Compound vs. WT	1.045	0.449
KEGG_BUTANOATE_METABOLISM	Acute ATL vs. Healthy	1.427	0.215	Compound vs. WT	1.206	0.261
KEGG_ADHERENS_JUNCTION	Acute ATL vs. Healthy	1.387	0.216	Compound vs. WT	0.766	0.852
KEGG_NOTCH_SIGNALING_PATHWAY	**Acute ATL vs. Healthy**	**1.399**	**0.224**	**Compound vs. WT**	**0.917**	**0.612**
KEGG_EPITHELIAL_CELL_SIGNALING_IN_HELICOBACTER_PYLORI_INFECTION	Acute ATL vs. Healthy	1.404	0.226	Compound vs. WT	1.022	0.471
KEGG_BETA_ALANINE_METABOLISM	Acute ATL vs. Healthy	1.350	0.239	Compound vs. WT	1.075	0.416
KEGG_N_GLYCAN_BIOSYNTHESIS	Acute ATL vs. Healthy	1.338	0.245	Compound vs. WT	1.093	0.399

Genesets with human FDR<0.25 and mouse FDR>0.25 are listed by decreasing order of humn FDR value. Metabolism-related pathways are colored. KEGG_NOTCH_SIGNALING_PATHWAY are displayed in bold.

Supplemental figure 1

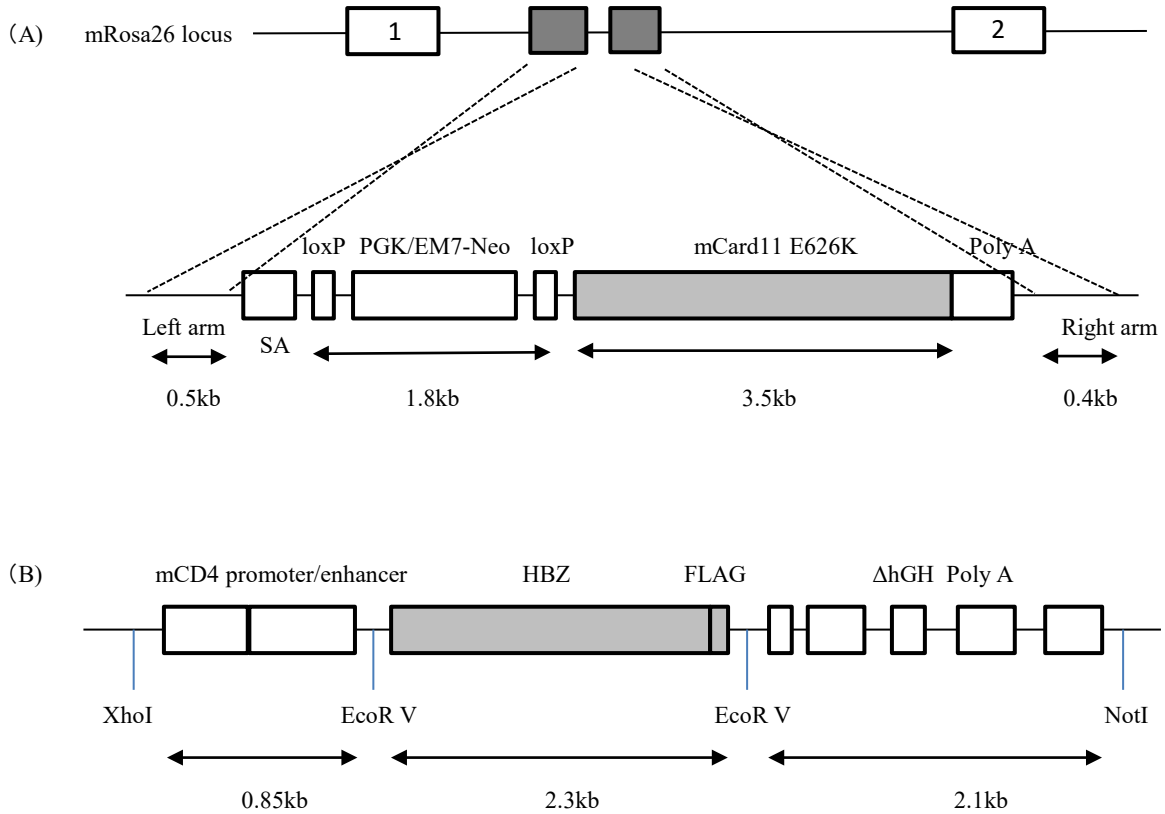

Supplemental figure 1. Strategy for targeting mutant mice.

(A) trategy for targeting CARD11(E626K)$^{stop\,FL}$ mice. *Card11*E626K cDNA, which is a murine homologue of human *CARD11*E616K, was inserted into the *mRosa26* vector, preceded by a loxP-flanked (FL) stop sequence. CARD11(E626K)$^{CD4\text{-}Cre}$ mice were obtained by crossing CARD11(E626K)$^{stop\,FL}$ mice with *CD4*-Cre transgenic (Tg) mice. SA, splice acceptor; loxP, loxP sequences; PGK, phosphoglycerate kinase eukaryotic promoter; EM7, EM7 prokaryotic promoter; Neo, neomycin resistance gene.

(B) Strategy for targeting *HBZ* Tg mice. The original transgene construct containing a mouse *CD4* promoter/enhancer, *vpr* (an accessory protein of HIV), and a defective human growth hormone gene with the polyadenylation signal were kindly provided by Dr. Iwakura from Tokyo University of Science(Yasuda et al., 2001). The *vpr* of the transgene construct was replaced by *HBZ-FLAG* after digestion with EcoRV and SmaI. The *HBZ* transgene construct was prepared for microinjection after digestion with XhoI and NotI.

Supplemental figure 2

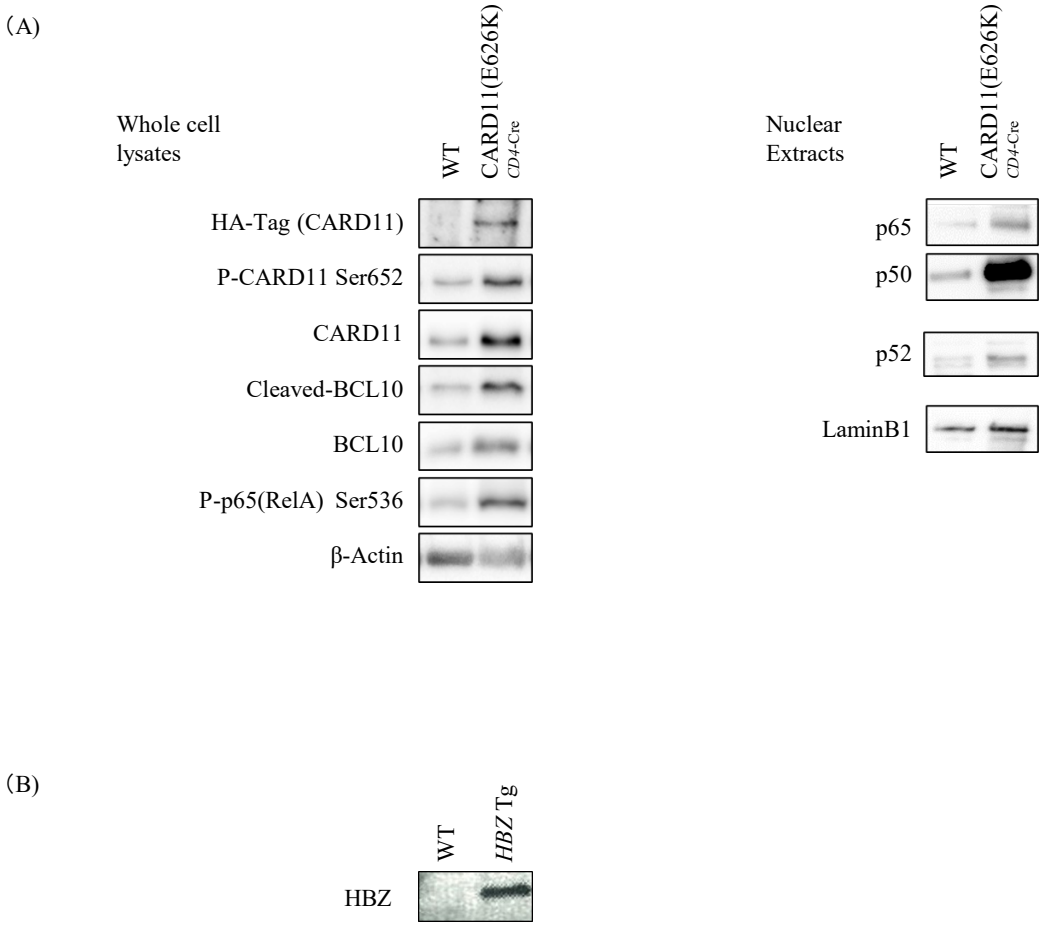

Supplemental figure 2. Western blot analysis of splenic CD4⁺ T cells from CARD11(E626K)$^{CD4\text{-}Cre}$ mice and *HBZ* Tg mice.

(A) Activation of the NF-κB pathway in CARD11(E626K)$^{CD4\text{-}Cre}$ mice. In total extract of splenic CD4⁺ T cells from CARD11(E626K)$^{CD4\text{-}Cre}$ mice, the amount of cleaved BCL-10 is increased compared with wild type (WT) CD4⁺ cells, while CARD11 Ser652 and NF-κB p65 Ser536 are phosphorylated in CARD11(E626K)$^{CD4\text{-}Cre}$ mice but not in WT CD4⁺ cells. As for the nuclear cell extracts, there are increments of p50, RelA p65, and p52, confirming the activation of both the canonical and non-canonical NF-κB pathways.
(B) HBZ expression in *HBZ* Tg mice. Total extracts from splenic CD4⁺ T cells were immunoprecipitated with anti-FLAG antibody and analyzed by western blot with anti-HBZ antibody. HBZ is detected in CD4⁺ T cells from *HBZ* Tg mice, but not those from WT mice.

Supplemental figure 3

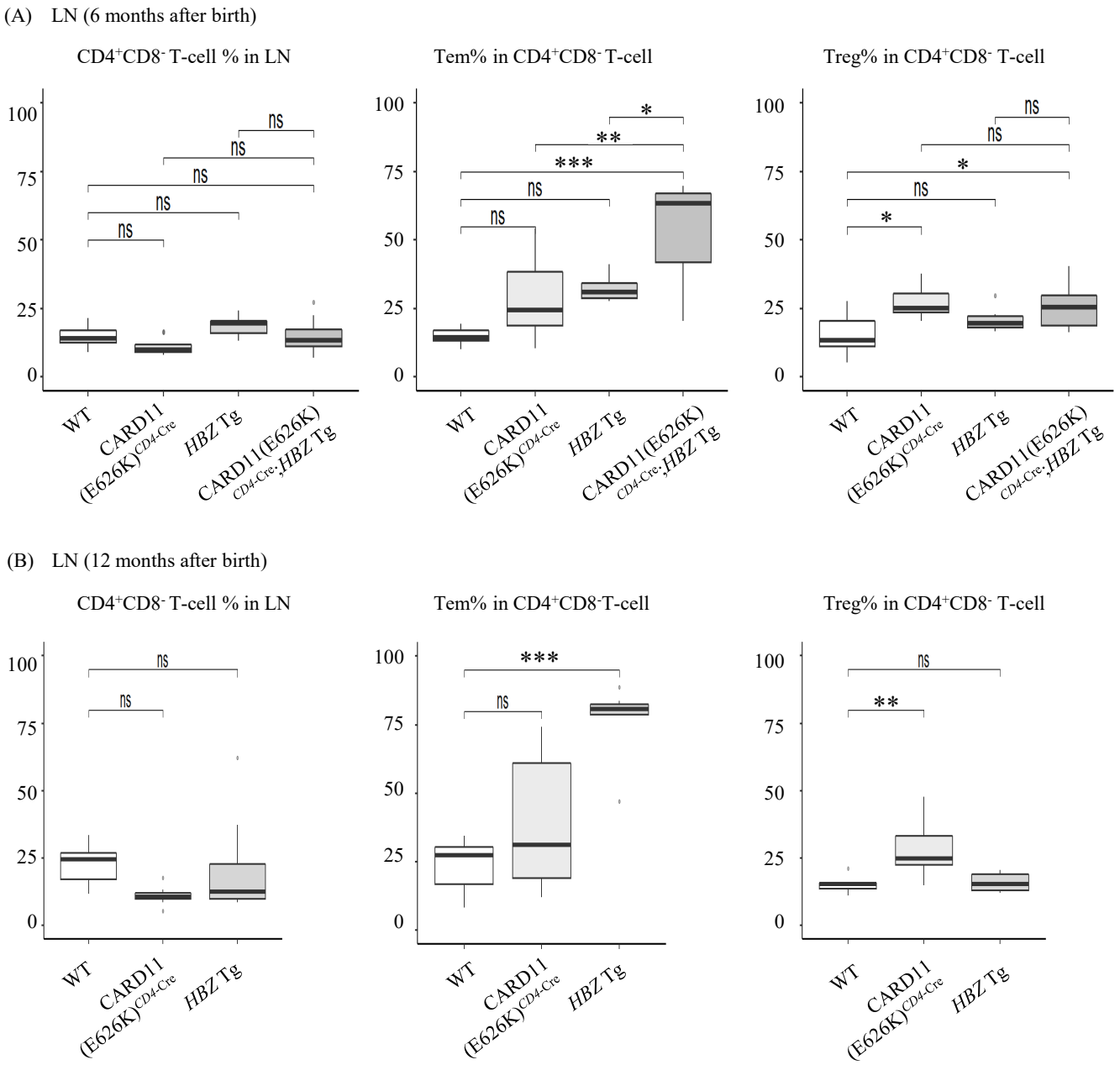

Supplemental figure 3. Abnormal increments of the relative percentages of effector/memory T cells and regulatory T cells in lymph nodes of CD4⁺ T cells in mutant mice.

The absolute percentage of lymph node (LN) $CD4^+CD8^-$ T cells, and the relative percentages of $CD4^+CD44^+CD62L^-$ effector/memory T cells (Tem%), and $CD4^+CD25^+$ regulatory T cells (Treg%) in the $CD4^+CD8^-$ T-cell subset. These absolute and relative percentages are shown at (A) 6 months after birth (wild type (WT), n = 6; CARD11(E626K)$^{CD4\text{-Cre}}$,n = 9; *HBZ* Tg, n = 7; and CARD11(E626K)$^{CD4\text{-Cre}}$;*HBZ* Tg, n = 9 mice) and at (B) 12 months after birth (WT, n = 5; CARD11(E626K)$^{CD4\text{-Cre}}$,n = 11; *HBZ* Tg, n = 8).

Abnormal relative percentages of T-cell subsets are observed at 6 and 12 months: in CARD11(E626K)$^{CD4\text{-Cre}}$ mice, Treg% increases at 6 and 12 months; in *HBZ* Tg mice, Tem increases at 12 months; in CARD11(E626K)$^{CD4\text{-Cre}}$;*HBZ* Tg mice, Tem% and Treg% increase at 6 months. In a comparison at 6 months, CARD11(E626K)$^{CD4\text{-Cre}}$;*HBZ* Tg mice show the most abnormal relative percentages of T-cell subsets. p values were calculated by the Tukey test after a one-way ANOVA; and *, **, *** represent p values less than 0.05, 0.01, and 0.001, respectively.

Supplemental figure 4

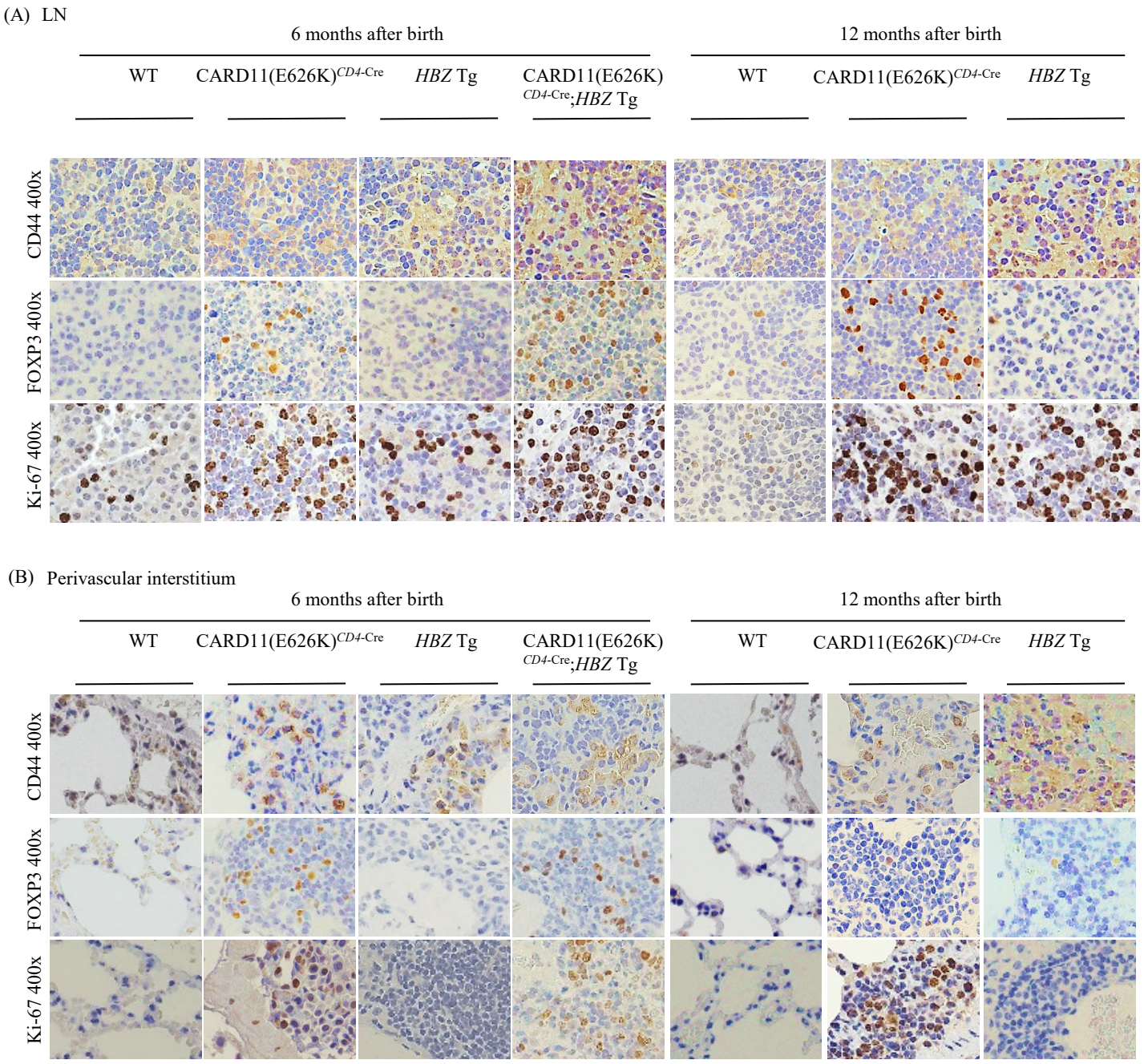

Supplemental figure 4. Identification of effector T cells, regulatory T cells, and proliferating cells in lymph nodes and lung of mutant mice.

Histologic analysis of the (A) lymph node (LNs) and (B) lung at 6 and 12 months after birth. Tissues were stained with anti-CD44, anti-FOXP3, and anti–Ki-67 antibodies.

(A) Distribution of CD44$^+$ effector T cells (Tem), FOXP3$^+$ regulatory T cells (Treg), and Ki-67$^+$ proliferating cells in LNs. In CARD11(E626K)$^{CD4\text{-Cre}}$ mice, Treg are increased at 6 and 12 months. In *HBZ* Tg mice, Tem cells are prominent at 12 months. In CARD11(E626K)$^{CD4\text{-Cre}}$;*HBZ* Tg mice, both Tem and Treg are increased at 6 months. Ki-67$^+$ cells comprise about 50% of LN cells of CARD11(E626K)$^{CD4\text{-Cre}}$;*HBZ* Tg mice, and this value is much higher than those in LN cells of CARD11(E626K)$^{CD4\text{-Cre}}$ and *HBZ* Tg mice.

(B) Infiltration of CD44$^+$ Tem, FOXP3$^+$ Treg, and Ki-67$^+$ proliferating cells into the lung perivascular interstitium. In CARD11(E626K)$^{CD4\text{-Cre}}$ mice, Treg have infiltrated the lung perivascular interstitium at 6 months. In *HBZ* Tg mice, Tem cells are prominent at 12 months. In CARD11(E626K)$^{CD4\text{-Cre}}$;*HBZ* Tg mice, both Tem and Treg are increased at 6 months. CARD11(E626K)$^{CD4\text{-Cre}}$;*HBZ* Tg mice show about 25%-50% higher indices of Ki-67$^+$ cells than CARD11(E626K)$^{CD4\text{-Cre}}$ and *HBZ* Tg mice.

Supplemental figure 5

(A)

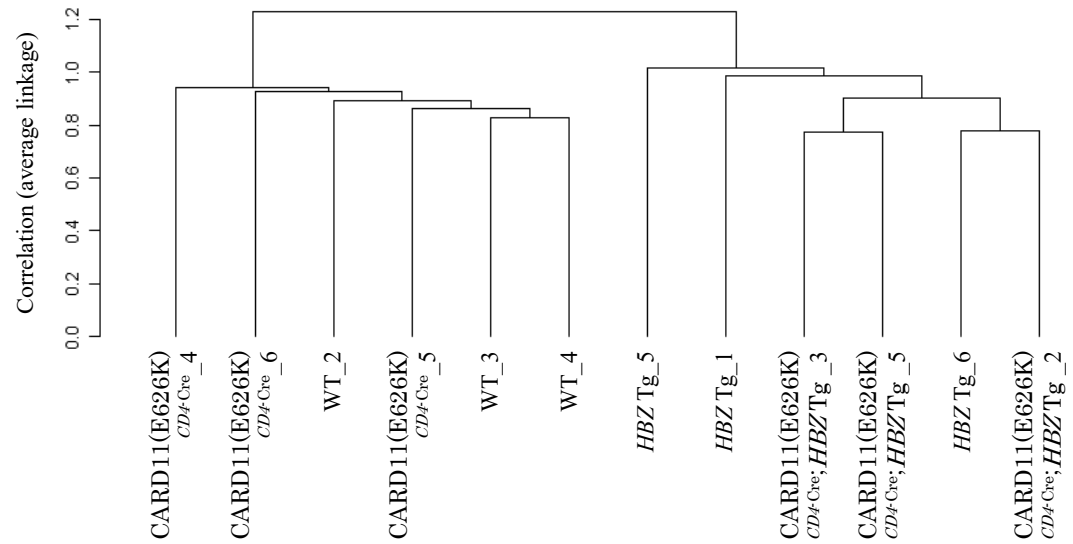

(B)

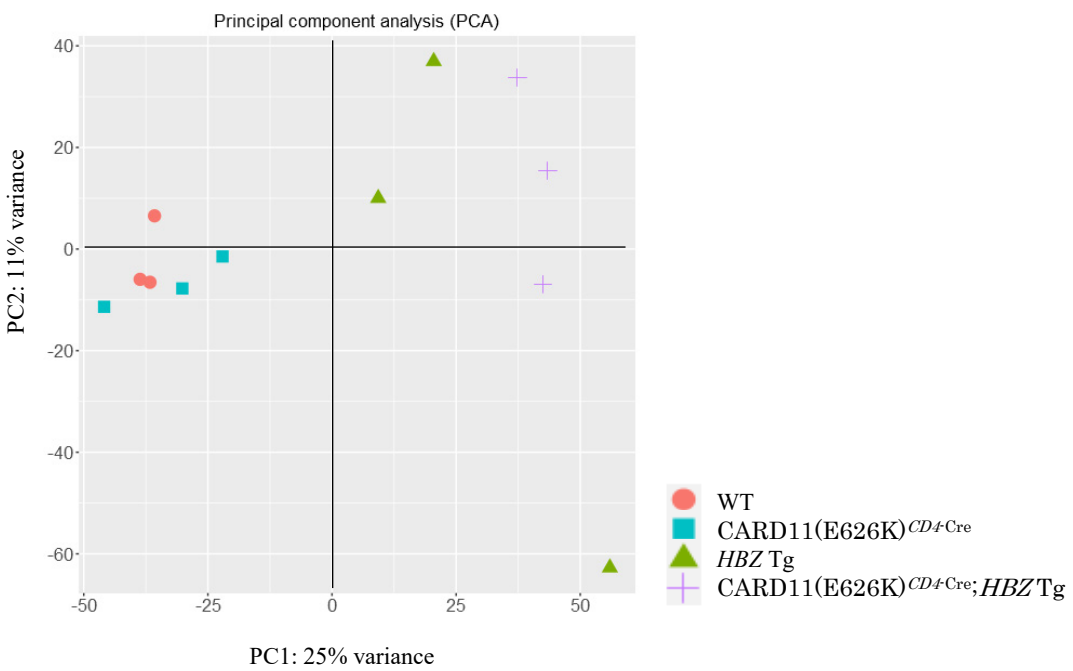

Supplemental figure 5. Global gene expression profiling of effector/memory T cells obtained from wild type, CARD11(E626K)$^{CD4\text{-}Cre}$, *HBZ* Tg, and CARD11(E626K)$^{CD4\text{-}Cre}$;*HBZ* Tg mice.

(A) Dendrogram constructed from unsupervised hierarchical clustering of RNA-seq data from 4 types of Tem using Pearson correlation. Tem from wild type (WT) and CARD11(E626K)$^{CD4\text{-}Cre}$ mice comprise one branch, and Tem from *HBZ* Tg and CARD11(E626K)$^{CD4\text{-}Cre}$;*HBZ* Tg mice comprise the other; this indicates that in CARD11(E626K)$^{CD4\text{-}Cre}$;*HBZ* Tg Tem, *HBZ* expression had greater effects on the global gene expression pattern than the CARD11 mutant.

(B) Principal component analysis of RNA-seq data from WT, CARD11(E626K)$^{CD4\text{-}Cre}$, *HBZ* Tg, and CARD11(E626K)$^{CD4\text{-}Cre}$;*HBZ* Tg Tem. The data shows that the CARD11 mutant and *HBZ* expression induced distinct transcriptomes.

Supplemental figure 6

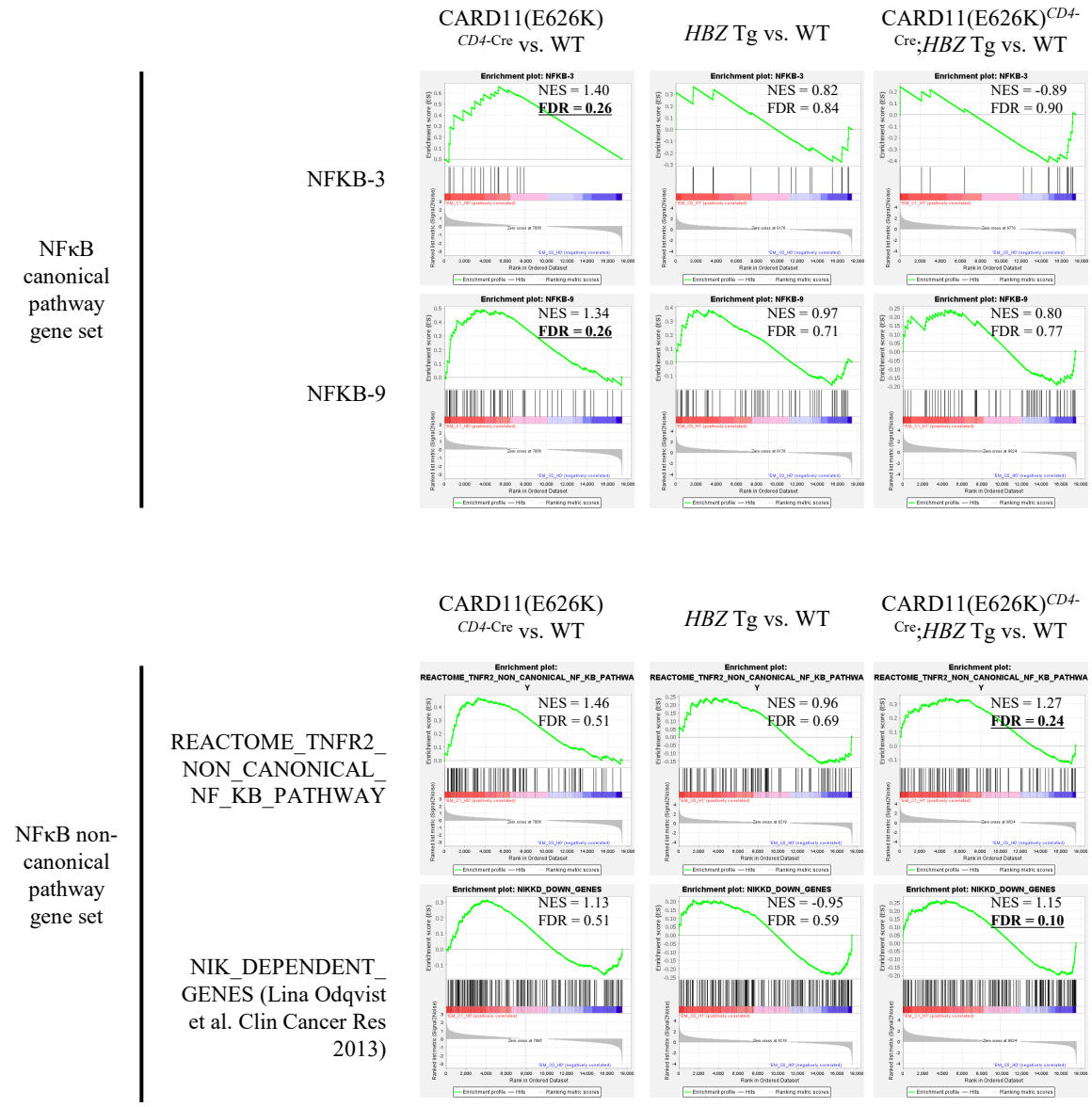

Supplemental figure 6. Activation of the NF-κB canonical signaling pathway in CARD11(E626K)*CD4*-Cre mice, and that of the NF-κB non-canonical signaling pathway in CARD11(E626K)*CD4*-Cre;*HBZ* Tg mice.

Gene set enrichment analysis (GSEA) of splenic $CD4^+CD44^+CD62L^-$ effector/memory T cells (Tem) from CARD11(E626K)*CD4*-Cre, *HBZ* Tg, and CARD11(E626K)*CD4*-Cre;*HBZ* Tg mice, compared with those from wild-type (WT) mice.

(A) Enrichment plots of NF-κB canonical pathway–related gene sets are shown with normalized enrichment scores (NESs) and false discovery rates (FDRs). NFKB-3 and NFKB-9 gene sets (SignatureDB), which are NF-κB canonical pathway gene sets, are positively enriched only in CARD11(E626K)*CD4*-Cre mice. NFKB-3 and NFKB-9 gene sets were defined as gene sets whose expressions were downregulated upon treatment with MLX105 and MLN120B, which are inhibitors of the canonical pathway molecule IkB kinase beta, respectively.

(B) Enrichment plot of NF-κB non-canonical pathway–related gene sets. REACTOME_TNFR2_NON_CANONICAL_NF_KB_PATHWAY (Molecular Signatures Database) and a gene set downregulated by the knockdown of non-canonical signaling molecule NF-κB–inducing kinase (NIK) (Odqvist et al., 2013) are positively enriched only in CARD11(E626K)*CD4*-Cre;*HBZ* Tg mice.

Supplemental figure 7

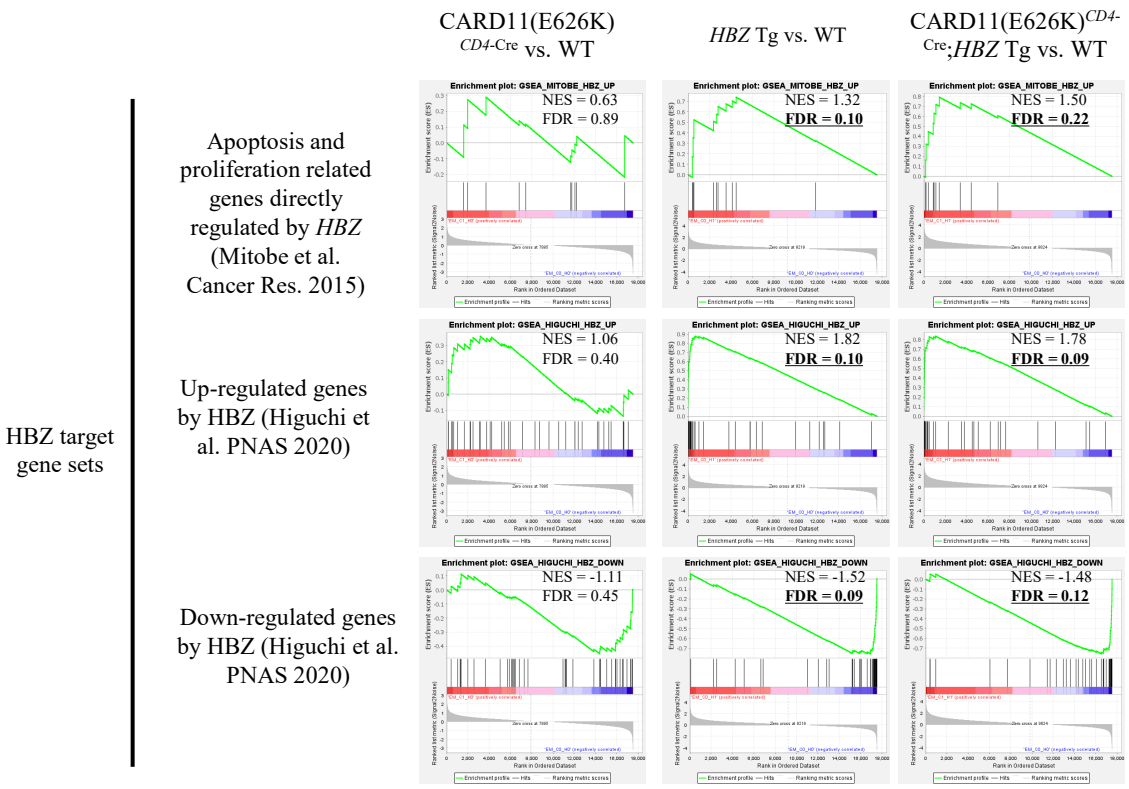

Supplemental figure 7. Dysregulation of HBZ target genes in *HBZ* Tg and CARD11(E626K)*CD4*-Cre;*HBZ* Tg mice.

Characteristic apoptosis- and proliferation-related genes that are directly upregulated by *HBZ mRNA* (Mitobe et al., 2015), including *AURKB, BUB1B, CCNA2, CCNB2, CENPH, MCM5, RAD51, RRM2, BIRC5 (Survivin),* and *TOP2A*, are enriched in both *HBZ* Tg mice and CARD11(E626K)*CD4*-Cre;*HBZ* Tg mice. Genes up- or downregulated by HBZ (Higuchi et al., 2015), including indirectly, are enriched in both *HBZ-Tg* and CARD11(E626K)*CD4*-Cre;*HBZ* Tg mice.